Directional filtering and side-swipe imaging

Ye Zheng and Robert R. Stewart

ABSTRACT

On seismic recordings, there may be some events from off-line reflectors (side-swipe). We could take advantage of these off-line energy to get a partial 3-D image from a 2-D line with 3 component seismic data. In this paper, a method of directional filtering and side-swipe imaging is presented. The least-squares method on time domain is used to determine the polarization degree and direction of the seismic signal. For P wave, the wave traveling direction is the same as the polarization direction. For S wave, the traveling direction is perpendicular to the polarization direction. This method is successfully applied to numerical models to separate in-line and off-line energy. After applying this method, we could get a better in-line imaging than that from conventional processing and could get a off-line image.

INTRODUCTION

Seismic recordings contain not only the reflections from points directly beneath the line, but also from areas on the sides of the line: We have both in-line and off-line energy. The existence of the off-line energy (French, 1974; Hospers, 1985) may result in the misinterpretation of conventional processed seismic data. If we can develop an algorithm to determine the direction of the incoming waves and to pass the waves from a specific direction, we could enhance the in-line energy and reject the off-line energy. This may improve the quality of the conventional section. The use of three component (3-C) seismic recordings allows this possibilities. Furthermore, we would like to take advantage of the recorded off-line energy to get the image of the off-line reflectors (Stewart, 1991; Ebrom, 1989). This means we could perhaps develop a partial 3-D image from a 2-D seismic line.

There have been a number of techniques developed to determine the polarization direction of seismic signals from multicomponent data (Flinn, 1965; Montalbetti and Kanasewich 1970, 1981; Jurkevics 1988; Samson, 1980, 1981 and Bataille, 1991). Most of polarization analysis relies on the eigenvalue method of analysing the covariance matrix of the observed data. The eigenvalues of the covariance matrix are related to the length of semi-axes of the polarization ellipse and the eigenvectors are related to the direction of the semi-axes. This is a good method to solve this problem, but much computation involved in the processing to get the eigenvalues and eigenvectors of the covariance matrix. Generally speaking, the more steps of computation involved, the more truncation error accumulated, and the more computer CPU time spent. Therefore, we developed a method which avoids constructing covariance matrix and save computation time involved the eigenvalue problem.

THE DIRECT LEAST-SQUARES METHOD

Let's discuss the 2-D problem. Assuming that the signal and noise are not correlated and the expectation value of the noise is zero, we define a seismic data set $\overrightarrow{V(t)} = (V_1(t),V_2(t))^T$ which contains signal as well as noise. Within a time window, we extract some data from $\overrightarrow{V(t)}$ as $\overrightarrow{u(t)} = (u_1(t),u_2(t))^T$, t=j-L, j+L, where j is the midpoint of the selected window and 2L+1 is the length of the window. The geometrical centre of the hodogram is:

$$x_0 = \frac{1}{2L+1}\sum_{t=j-l}^{j+l} u_1(t)$$

$$y_0 = \frac{1}{2L+1}\sum_{t=j-l}^{j+l} u_2(t) \qquad (1)$$

Assuming there is a line through the centre of the hodogram (x_0, y_0) with the direction cosine (cos θ, sin θ). We can project the displacement vector to the line and sum up the squares of the projection:

$$A(\theta) = \sum_{t=j-l}^{j+l} \left((u_1(t)-x_0)\cos\theta + (u_2(t)-y_0)\sin\theta\right)^2 \qquad (2)$$

If the line has the same direction as the major axis of the polarization ellipse, A receives its maximum value. If the line has the same direction of the minor axis of the ellipse, A receives its minimum value. To get the direction of the line making A maximum or minimum, let:

$$\frac{dA(\theta)}{d\theta} = 2\sum_{t=j-l}^{j+l} \left(-(u_1(t)-x_0)\sin\theta + (u_2(t)-y_0)\cos\theta\right)\left((u_1(t)-x_0)\cos\theta + (u_2(t)-y_0)\sin\theta\right)$$

$$= 0 \qquad (3)$$

After a few mathematical manipulations, we get:

$$\tan 2\theta = \frac{2\psi_{12}}{\psi_{22} - \psi_{11}} \qquad (4)$$

Where, $\psi_{11} = \sum_{t=j-l}^{j+l} (u_1(t)-x_0)^2$

$$\psi_{22} = \sum_{t=j-l}^{j+l} (u_2(t)-y_0)^2$$

$$\psi_{12} = \sum_{t=j-l}^{j+l} (u_1(t)-x_0)(u_2(t)-y_0)$$

It can be verified that if $\frac{dA(\theta)}{d\theta}$ is 0, $\frac{dA(\theta\pm\frac{\pi}{2})}{d\theta}$ and $\frac{dA(\theta\pm\pi)}{d\theta}$ are also 0. We prove $\frac{dA(\theta+\frac{\pi}{2})}{d\theta} = 0$ as an example. Substituting $\theta+\frac{\pi}{2}$ for θ, it becomes:

$$\frac{d(\theta+\frac{\pi}{2})}{d\theta} = 2\sum_{t=j-l}^{j+l} \left\{ \left(-(u_1(t)-x_0)\sin\left(\theta+\frac{\pi}{2}\right) + (u_2(t)-y_0)\cos\left(\theta+\frac{\pi}{2}\right)\right) \cdot \left((u_1(t)-x_0)\cos\left(\theta+\frac{\pi}{2}\right) + (u_2(t)-y_0)\sin\left(\theta+\frac{\pi}{2}\right)\right) \right\}$$

$$= 2\sum_{t=j-l}^{j+l} \left\{ \left(-(u_1(t)-x_0)\cos\theta - (u_2(t)-y_0)\sin\theta\right) \cdot \left(-(u_1(t)-x_0)\sin\theta + (u_2(t)-y_0)\sin(\cos\theta)\right) \right\}$$

$$= -\frac{dA(\theta)}{d\theta} = 0 \qquad (5)$$

It is also true that $A(\theta\pm\pi)$ equals $A(\theta)$.

$$A(\theta\pm\pi) = \sum_{t=j-l}^{j+l} \left((u_1(t)-x_0)\cos(\theta\pm\pi) + (u_2(t)-y_0)\sin(\theta\pm\pi)\right)^2$$

$$= \sum_{t=j-l}^{j+l} \left(-((u_1(t)-x_0)\cos\theta + (u_2(t)-y_0)\sin\theta)\right)^2$$

$$= \sum_{t=j-l}^{j+l} \left((u_1(t)-x_0)\cos\theta + (u_2(t)-y_0)\sin\theta\right)^2 = A(\theta) \qquad (6)$$

After we get θ from equation 4, we should compare $A(\theta)$ and $A(\theta+\frac{\pi}{2})$. The direction associated with the larger A is the direction of the major axis of the ellipse, and the smaller correspondents to the minor axis.

Assuming $A_1=A(\theta)$ is greater than $A_2=A(\theta+\frac{\pi}{2})$, we define the first filter factor as:

$$G_1 = 1 - A_2/A_1 \tag{7}$$

G_1 varies between 0 and 1. For a rectilinear wave, the hodogram should be a line. Therefore the projection of the displacement vector on the line perpendicular to the hodogram line is 0. A_2 is 0 and G_1 is 1. For circular polarized wave, the projection of the displacement vector on the line of any direction will same. Therefore, A_1 equals A_2 and G_1 is 0.

The direction vector of the major axis of the ellipse is $\vec{e_1} = (\cos\theta, \sin\theta)^T$, so the second filter factor is:

$$\vec{G_2} = \left|\vec{u(j)} \cdot \vec{e_1}\right| \vec{e_1} = g\,(\cos\theta, \sin\theta)^T \tag{8}$$

Where, $g = \left|u_1(j)\cos\theta + u_2(j)\sin\theta\right|$.

If we want to pass the waves within a certain range of directions, the directional filter factor is defined as following:

$$G_3 = \begin{cases} 1, \text{ if } \theta_0-\varphi \le \theta \le \theta_0+\varphi \\ 0, \text{ if } \theta \le \theta_0-\varphi \text{ or } \theta \ge \theta_0+\varphi \end{cases} \tag{9}$$

Where, θ_0 is the midpoint of the direction window. φ is the half-length of the window.

The output of the filter for passing the waves of the direction within the window of $\theta_0-\varphi \le \theta \le \theta_0+\varphi$ is:

$$\vec{u'} = G_1\vec{G_2}G_3 = (1-A_2/A_1)\, g\, G_3\, (\cos\theta, \sin\theta)^T \tag{10a}$$

For rejecting the waves of the direction within the window, the output of the filter is:

$$\vec{u'} = G_1\vec{G_2}(1-G_3) = (1-A_2/A_1)\, g\, (1-G_3)\, (\cos\theta, \sin\theta)^T \tag{10b}$$

Of course, some other smoothing function could be applied to the filter factors.

APPLICATION TO NUMERICAL MODELS

Two models are used in this study. One is the 'Fault Model' (Figure 1) and another is the 'Dome Model' (Figure 2). Both models are one-layer models. The P-wave velocity of the layer is 2000 m/s and the velocity under the layer is 2700 m/s. The geometry (Figure 3) of the seismic line is same for the two models except the distance from the line to the off-line reflector. The line runs from north to south with 1000 m long. There are total 51 geophones with the spacing of 20 m. A total of 11

shots are recorded by all geophones. The shot spacing is 100 m. The trace on the shot point location is not recorded, giving rise to 50 trace records. The recorded time is 1000 ms and the sampling interval is 2 ms.

Fault Model

The raw data are shown on Figure 4. We have added 15% noise on the record. The stacked section of vertical component using conventional processing is shown on Figure 5. We can see that we have two events in the section. We applied the directional filter to enhance the in-line energy. The stacked section of the in-line energy enhanced data is shown on Figure 6. There is only one reflection which is from the flat interface beneath the line. The directional filter is also applied to reject the in-line energy and to enhance the off-line energy. The stacked section of the off-line energy enhanced data is shown on Figure 7. We got the image of the off-line reflection.

Dome Model

The raw data with 12% noise is on Figure 8. The migrated section of the raw data is shown on Figure 9. The migrated section of in-line energy enhanced data is shown on Figure 10. The migrated section of the off-line energy enhanced data is shown on Figure 11. From the result of the processing, we can find that on the off-line enhanced section, the dome is highlighted and the in-line energy is eliminated obviously. The migrated section of the in-line enhanced data is better that the migrated section of the raw data using conventional method.

The suggested procedure of the off-line imaging is: (1) first, use conventional processing on vertical component of the seismic recording, (2) pass the 3-C data into the directional filter to reject the in-line energy, (3) use the velocity from the first step to process the vertical component the directional filtered data to get a rough image of the off-line energy. (4) use some narrow direction band to filter the raw data and to get more accurate off-line image. When we process the directional filtered data, we may adjust the velocity structure we got from the first step, because the length of the raypath for in-line and off-line reflections are different.

CONCLUSIONS AND FUTURE WORK

Directional filtering for 3-component seismic data is possible. We have successfully applied the filter to process synthetic data. Off-line energy is extracted from the data and separated from the in-line energy. The off-line energy is highlighted on the filtered section. And the location of the off-line reflector could be estimated.

In order to apply this technique on the real data, the following work should be done in the future:
(1) Multilayer synthetic modeling;
(2) Physical modeling;
(3) Effect of the free surface.

We also plan to apply directional filtering and off-line imaging technique on real data, Sikanni data (Figures 12) of Imperial Oil and Rumsey data (Figures 13) of Gulf Canada. The Sikanni data are very noisy and there is little coherence on raw data. On the bandpass (15-20-45-50) filtered data, we can see some signals. The Rumsey data

are better than the Sikanni data. Both data are three component data. We expect to get more information with the directional filtering than that with conventional processing.

ACKNOWLEDGEMENTS

The authors would like to thank all CREWES sponsors for supporting our research, and Imperial Oil, BFR Geophysical Ltd. and Gulf Canada for releasing the real data.

REFERENCES

Bataille, K. and Chiu, J.M., 1991, Polarization analysis of high-frequency, three-component seismic data: Bull. Seis. Soc. Am., **81**, 622 - 642.

Ebrom, D.A., Tatham, R.H., Sekheren, K.K., McDonald, J.A. and Gardner, G.H.F., 1989, Nine-component data collection over a reflection dome: A physical modeling study: presented at the 59th Ann. Internat. Mtg., Soc. Expl. Geophys.

Flinn, E.A., 1965, Signal analysis using rectilinearity and direction of particle motion: Proc. I.E.E.E., **53**, 1874 - 1876.

French, W.S., 1974, Two-dimensional and three-dimensional migration of model-experiment reflection profiles: Geophysics, **39**, 265 - 277.

Hospers, J., 1985, Sideswipe reflections and other external and internal reflections from salt plugs in the Norweigian-Danish basin: Geophys. Prosp., **33**, 52 - 71.

Jurkevics, A., 1988, Polarization analysis of three-component array data: Bull. Seis. Soc. Am., **78**, 1725 - 1743.

Kanasewich, E.R., 1981, Time sequence analysis in geophysics; The University of Alberta Press.

Montalbetti, J.F., and Kanasewich, E.R., 1970, Enhancement of teleseismic body phases with a polarization filter: Geophys. J.R. Astro. Soc., **21**, 119 - 129.

Samson, J.C., and Olson, J.V., 1980, Some comments on the descriptions of the polarization state of waves: Geophys. J.R. Astro., **61**, 115 - 130.

Samson, J.C., and Olson, J.V., 1981, Data-adaptive polarization filters for multichannel geophysical data: Geophysics, **46**, 1423 - 1431.

Stewart, R.R. and Machisio, G., 1991, Side-scanning seismic: Analysis and a physical modeling study: Presented at the 1991 Ann. Nat. Mtg., Can. Soc. Expl. Geophys., Calgary.

Stewart, R.R., 1991, Directional filtering using multicomponent seismic arrays: CREWES Project Research Report, Vol. 3.

Yilmaz, O., 1987, Seismic data processing: Soc. Expl. Geophys.

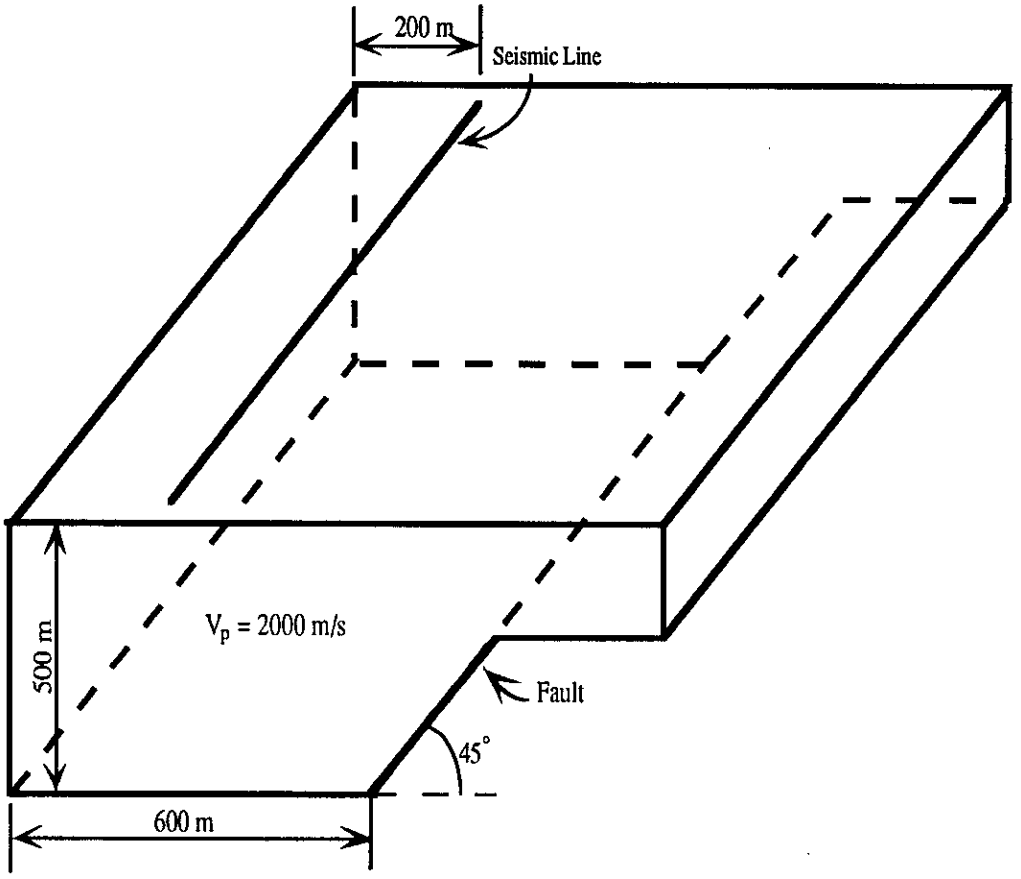

FIG 1: **Fault Model**. The seismic line is 1000 m long. There are 51 geophones and 11 shots. Two reflections are recorded. One is from the flat interface beneath the line and another is from the fault.

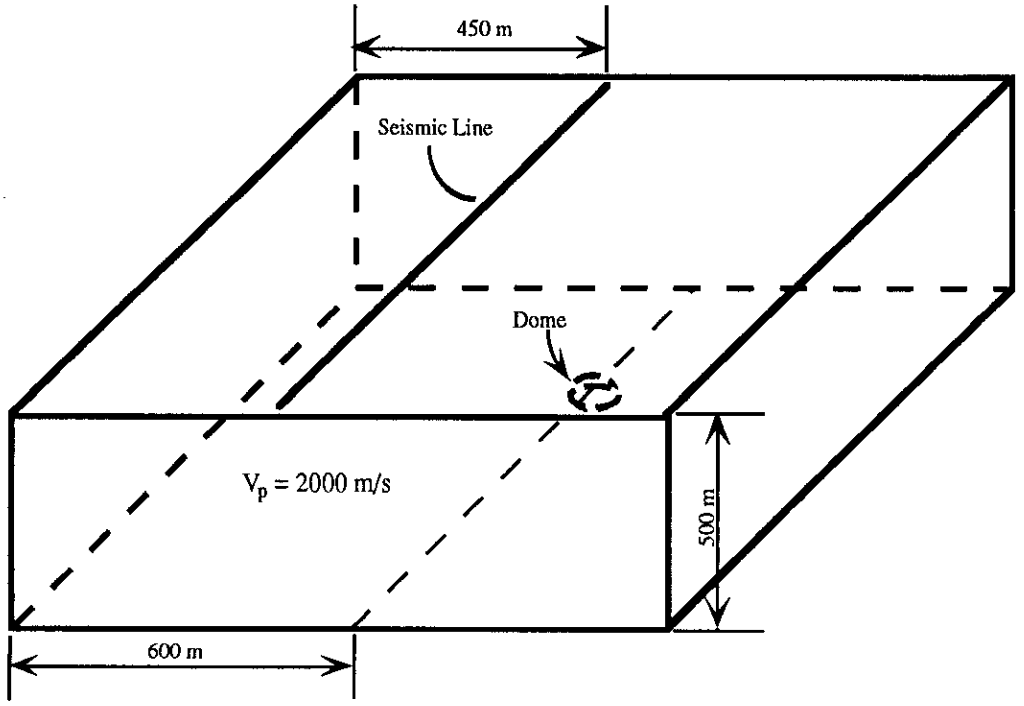

FIG 2: **Dome Model.** The geometry of the line is the same as that in Figure 1. Besides the reflection from the flat interface beneath the line, there will some scattered wave from the dome recorded on the seismic data.

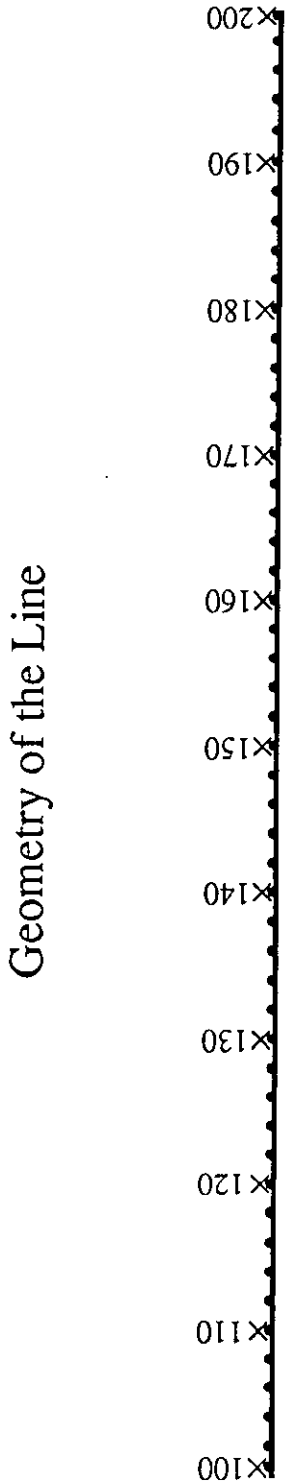

FIG 3: The geometry of the seismic line used for both the Fault Model and the Dome Model. The shot spacing is 50 m and the geophone spacing is10 m.

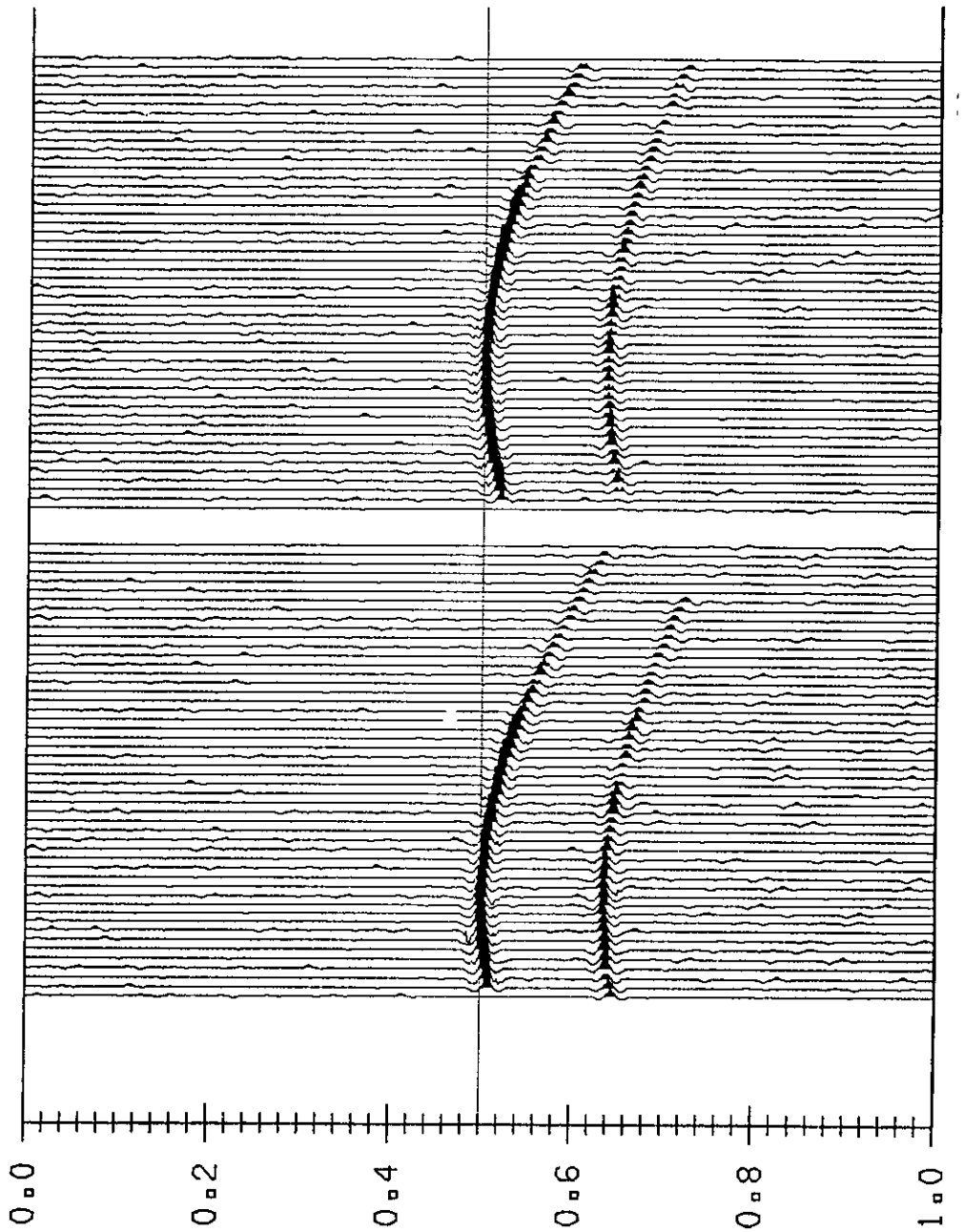

FIG 4a: Vertical component records from the **Fault Model**.

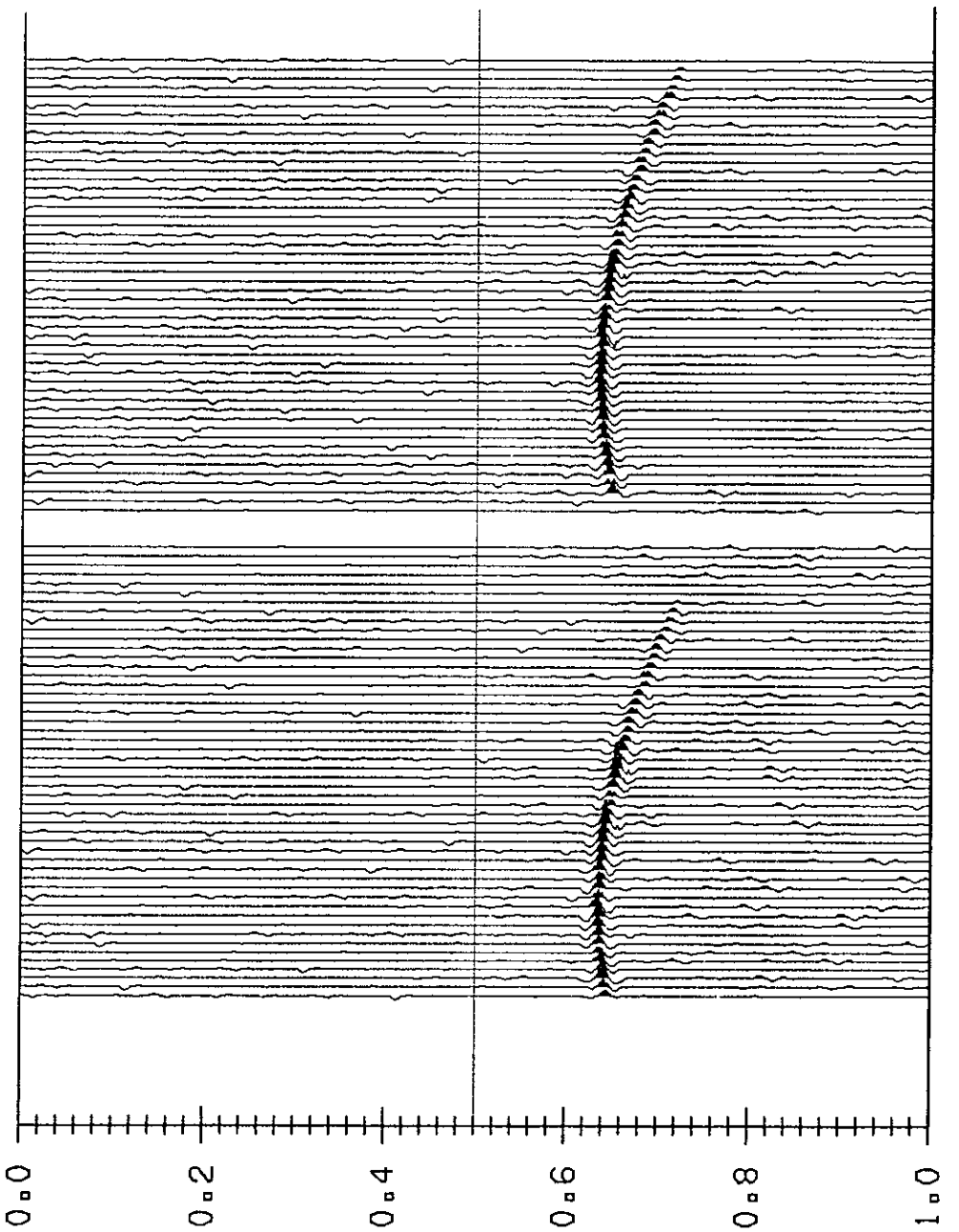

FIG 4b: Transverse component records from the **Fault Model.**

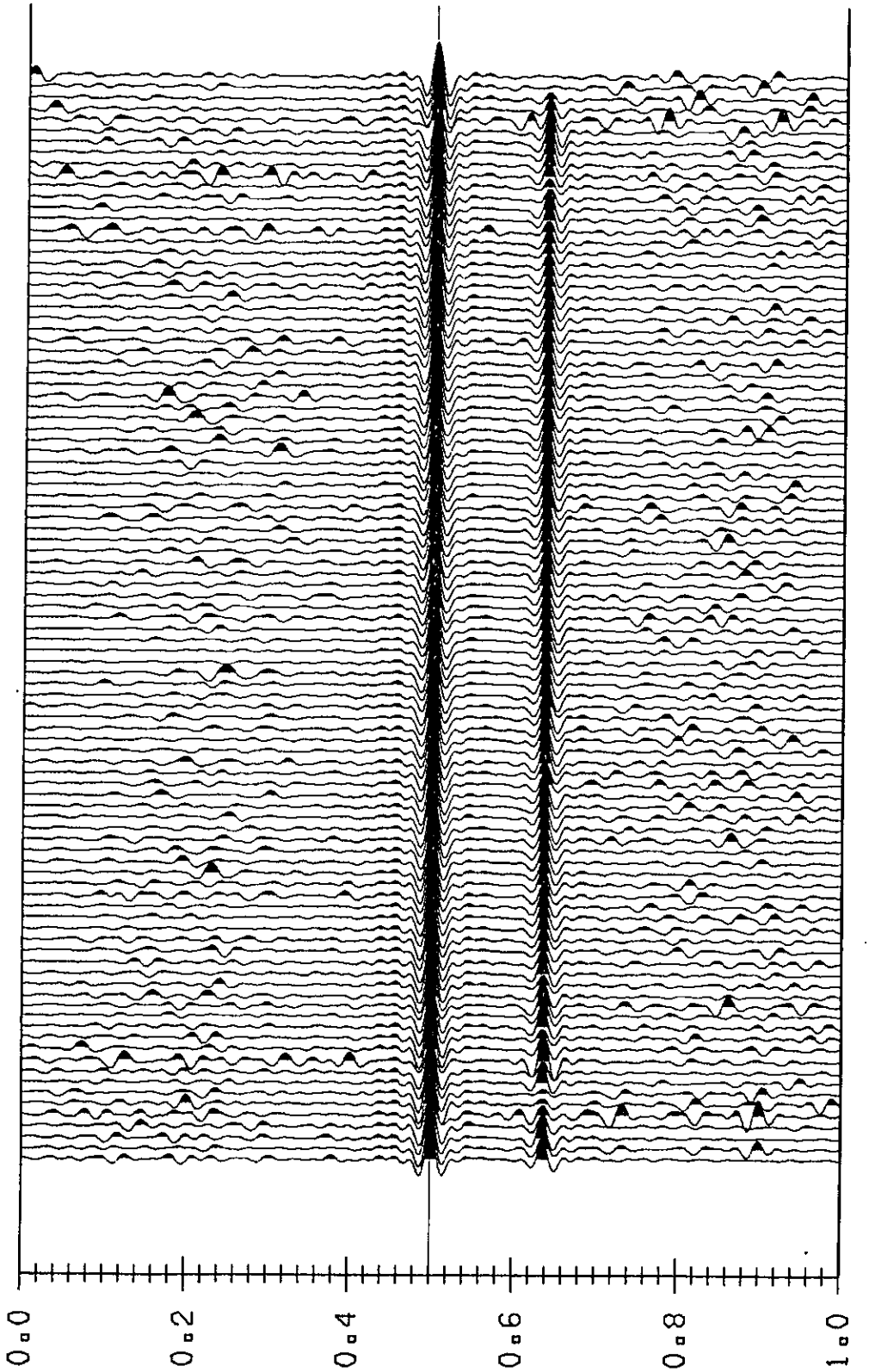

FIG 5: Stacked section of the vertical component data using conventional method (Fault Model).

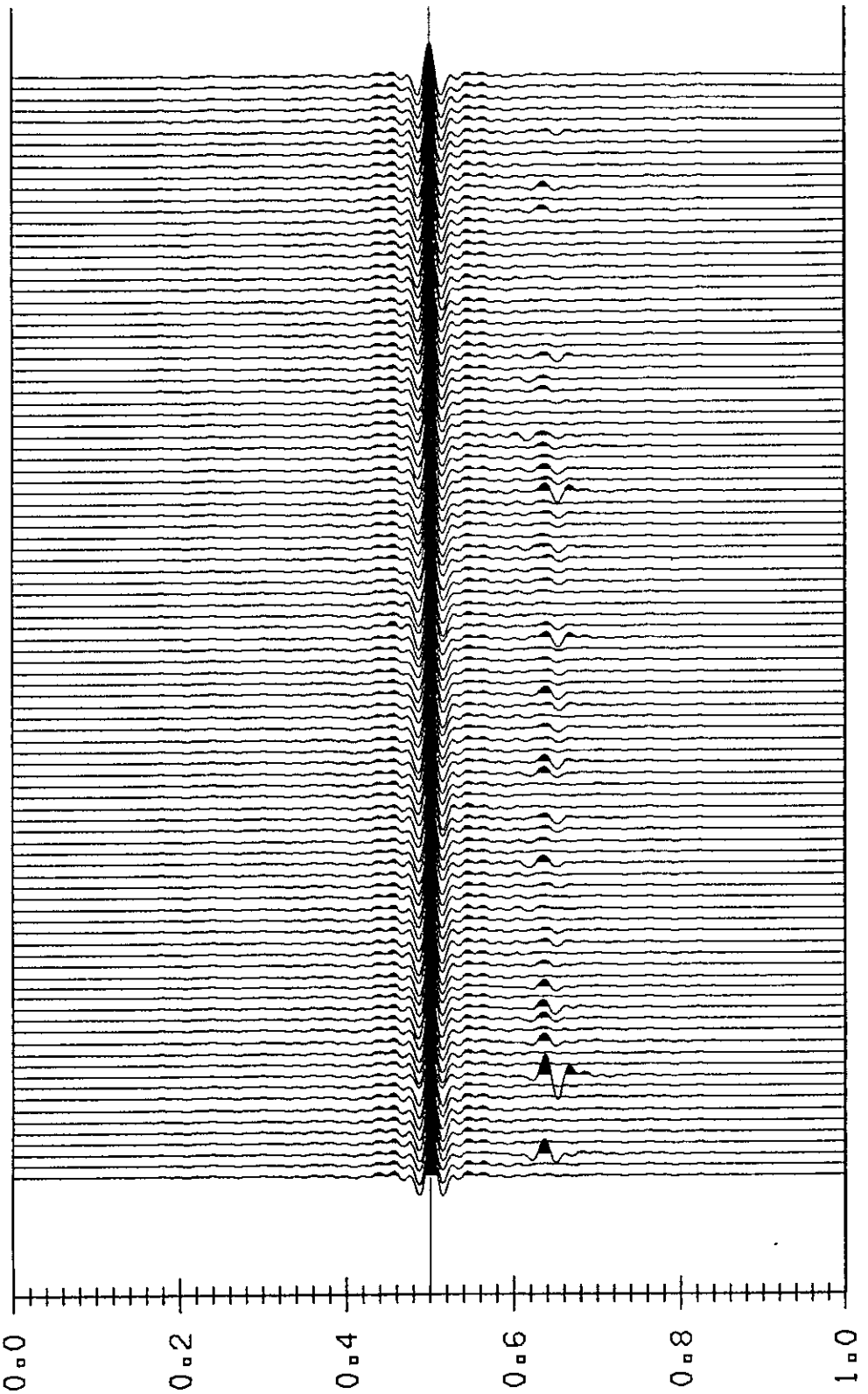

FIG 6: Stacked section of the vertical component of the off-line energy suppressed data (Fault Model).

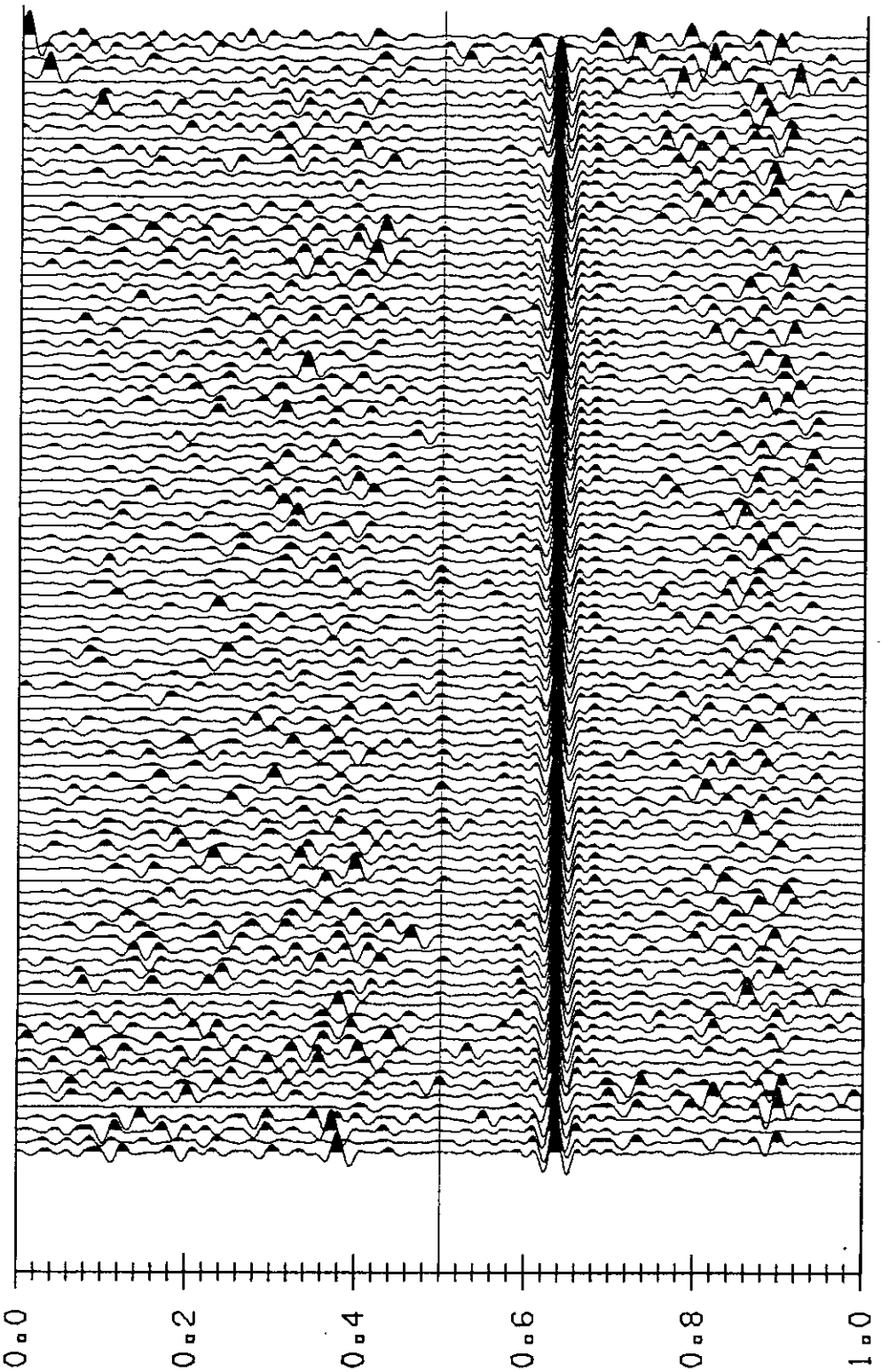

FIG 7: Stacked section of the vertical component of the off-line energy enhanced data (Fault Model).

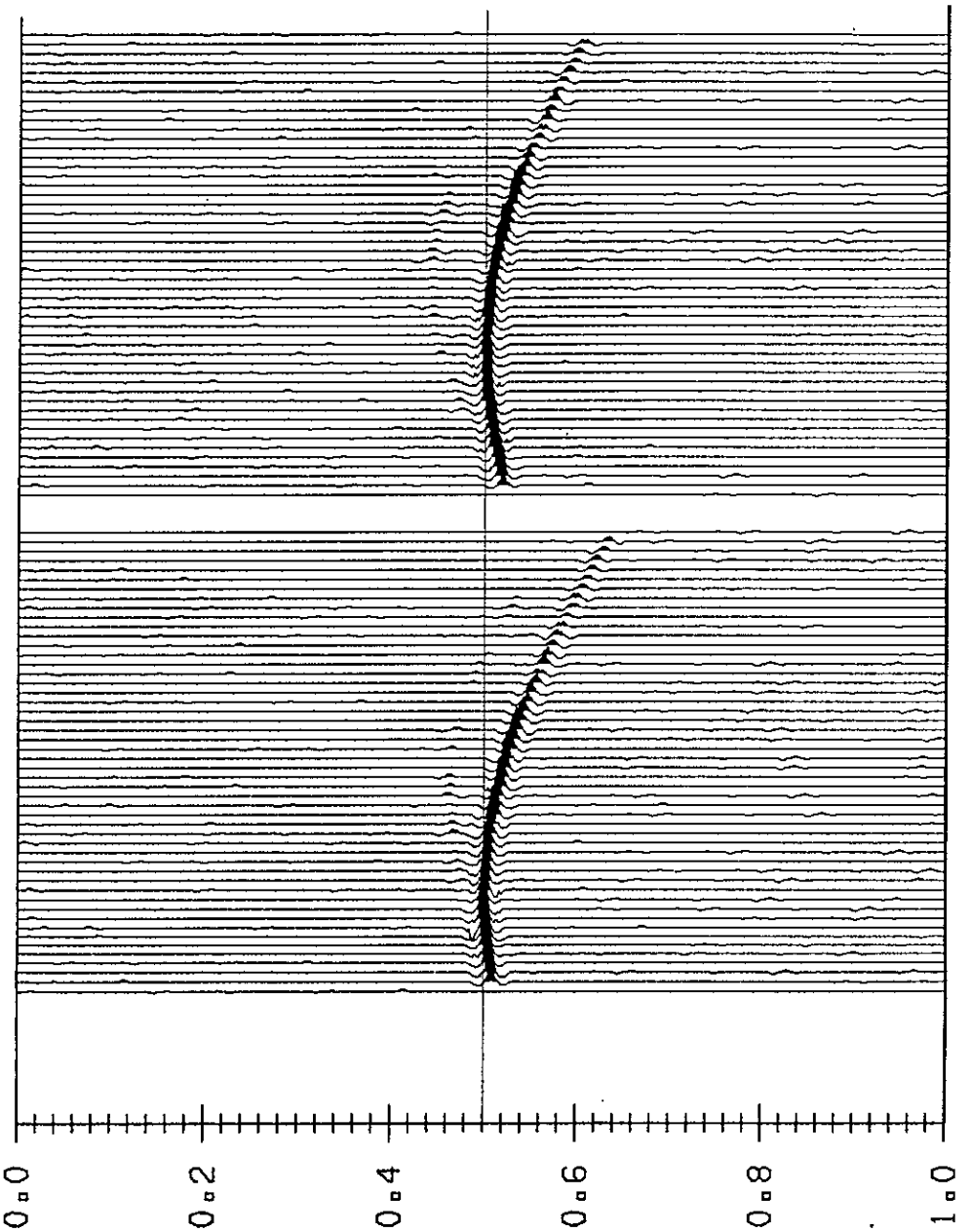

FIG 8a: Vertical component records from the **Dome Model.**

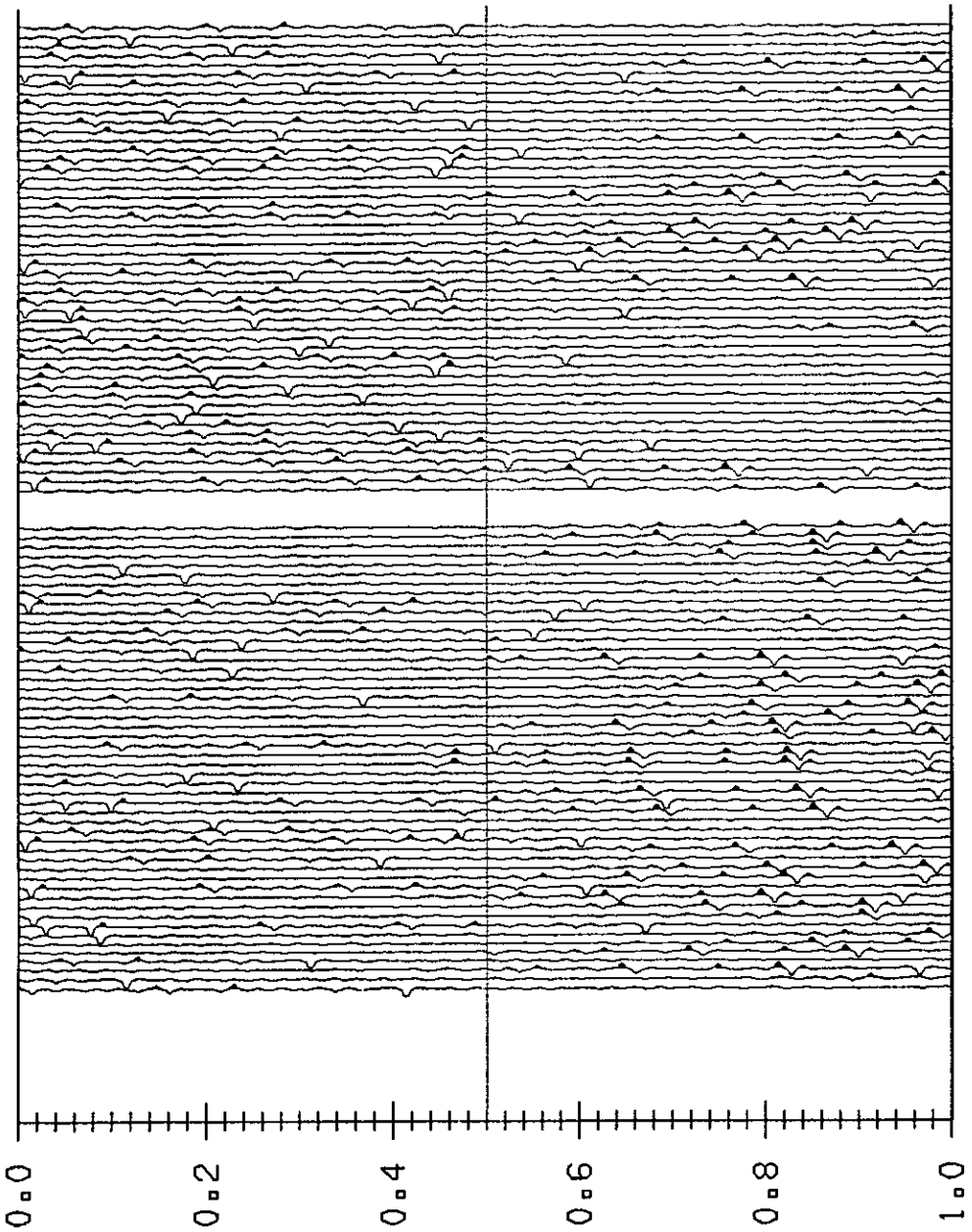

FIG 8b: Transverse component records from the **Dome Model.**

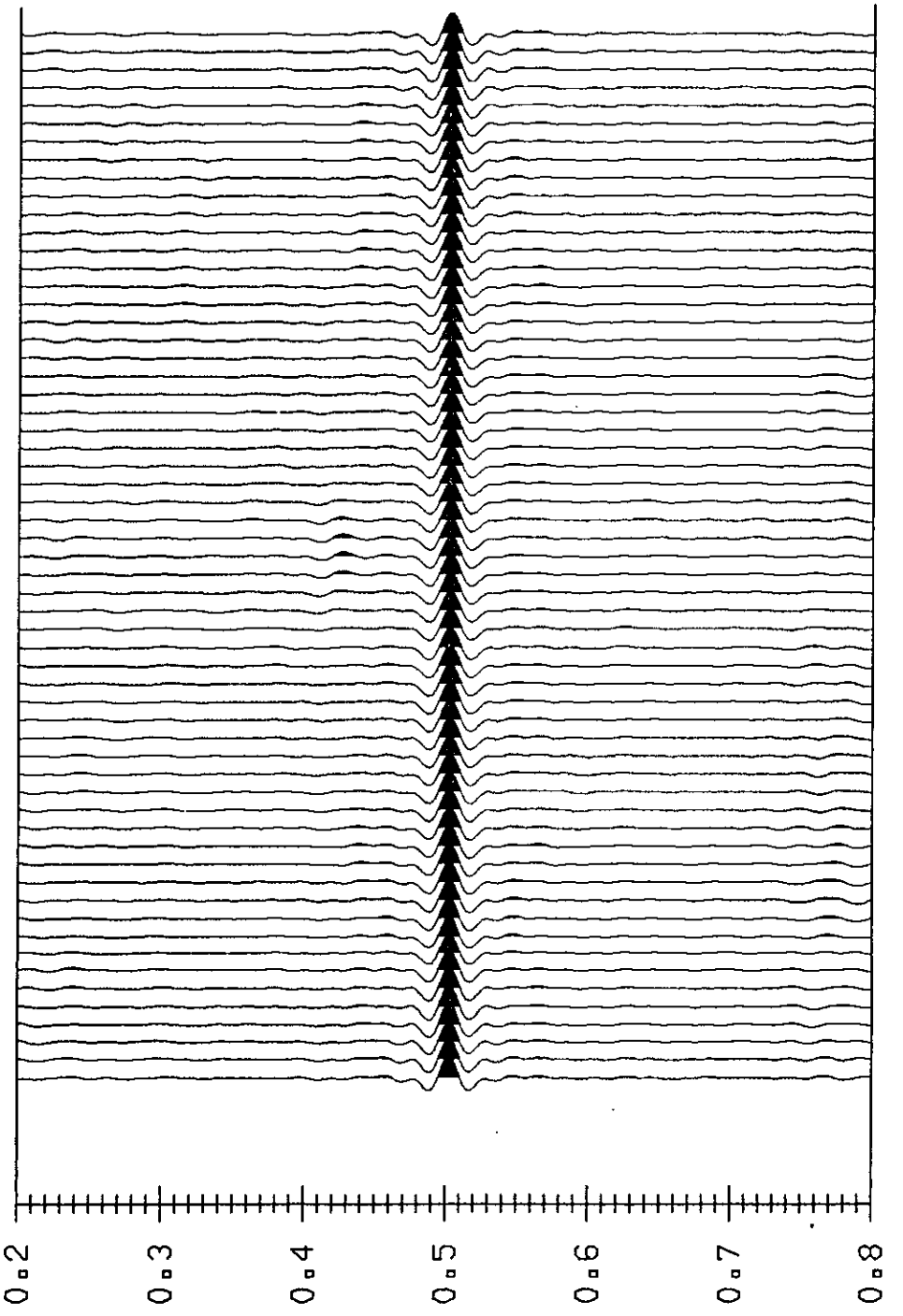

FIG 9: Migrated section of the vertical component data using conventional method (Dome Model).

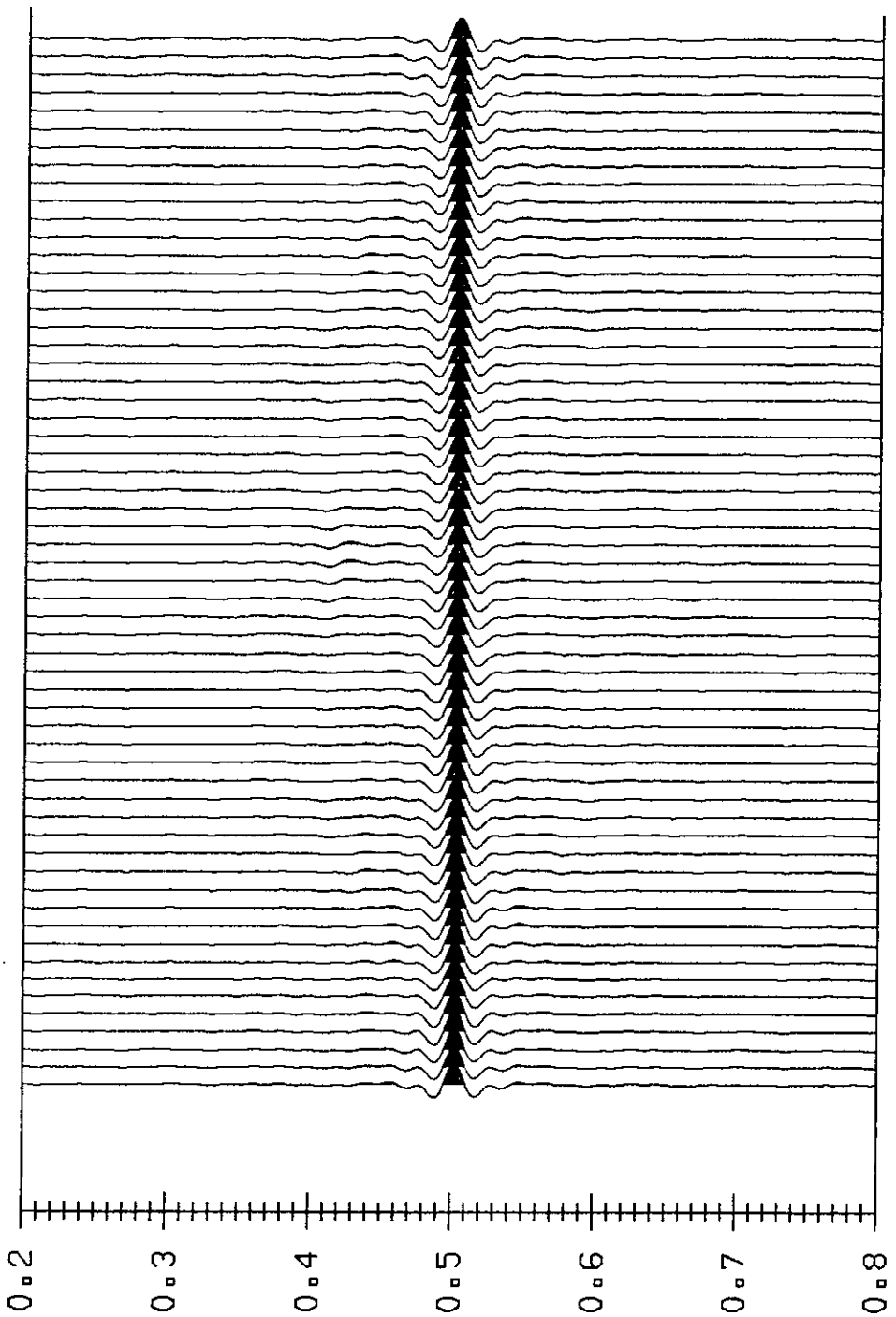

FIG 10: Migrated section of the vertical component of the in-line energy enhanced data (Dome Model).

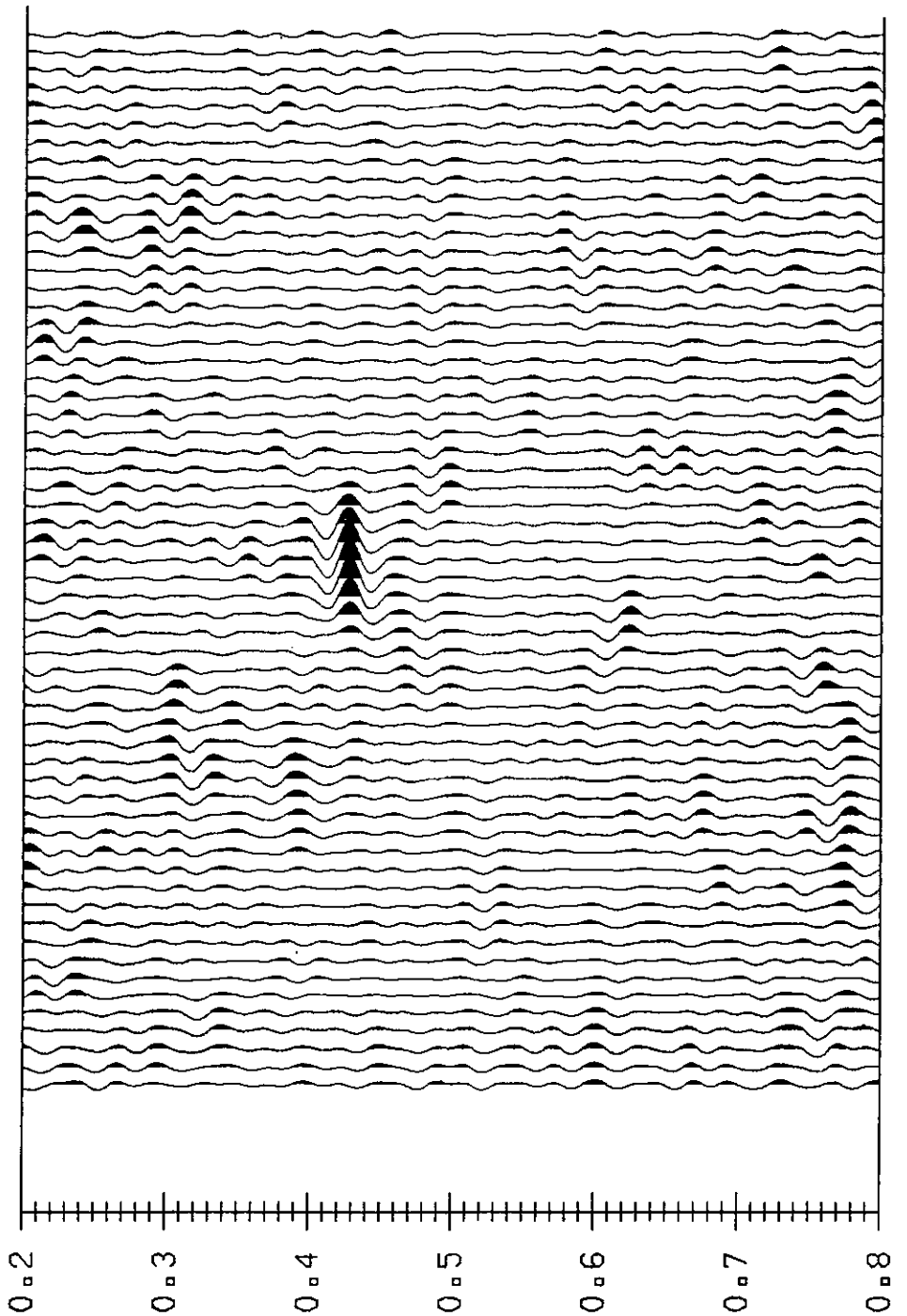

FIG 11: Migrated section of the vertical component of the off-line energy enhanced data (Dome Model).

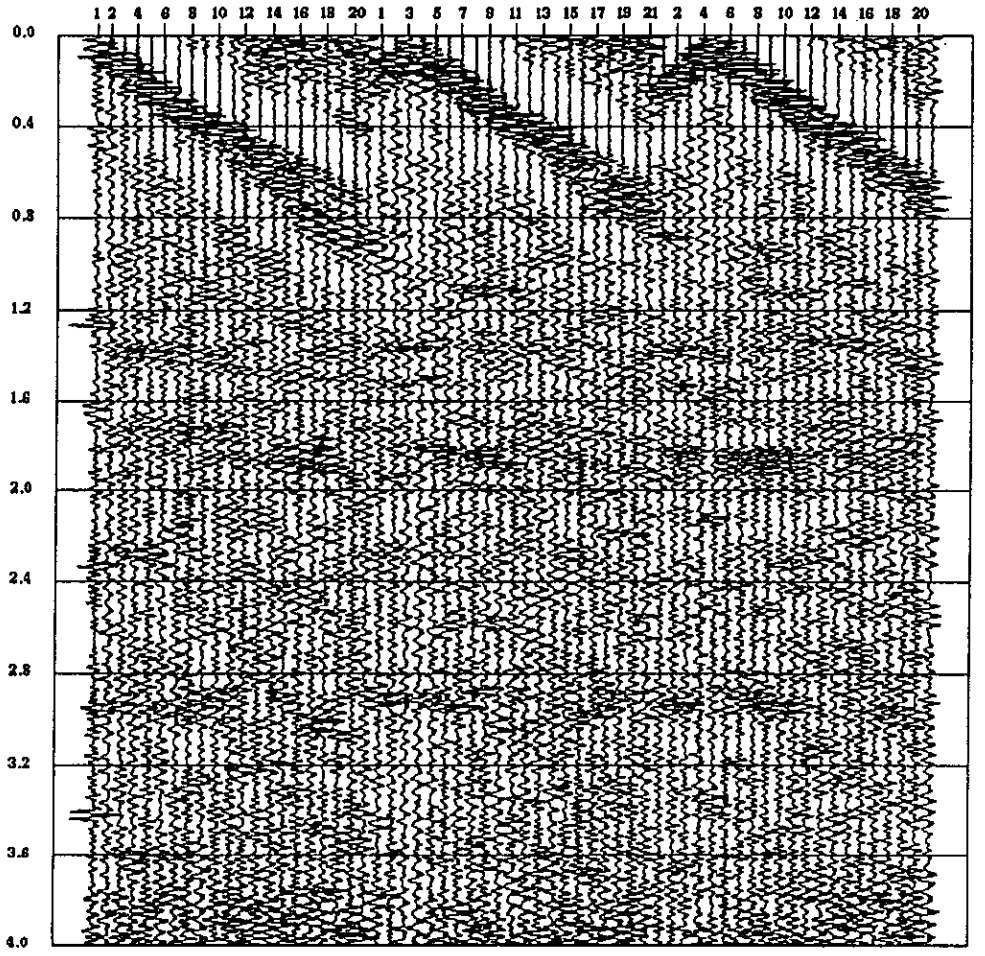

FIG 12. The bandpass filtered (15-20-45-50) vertical component of Sikanni data

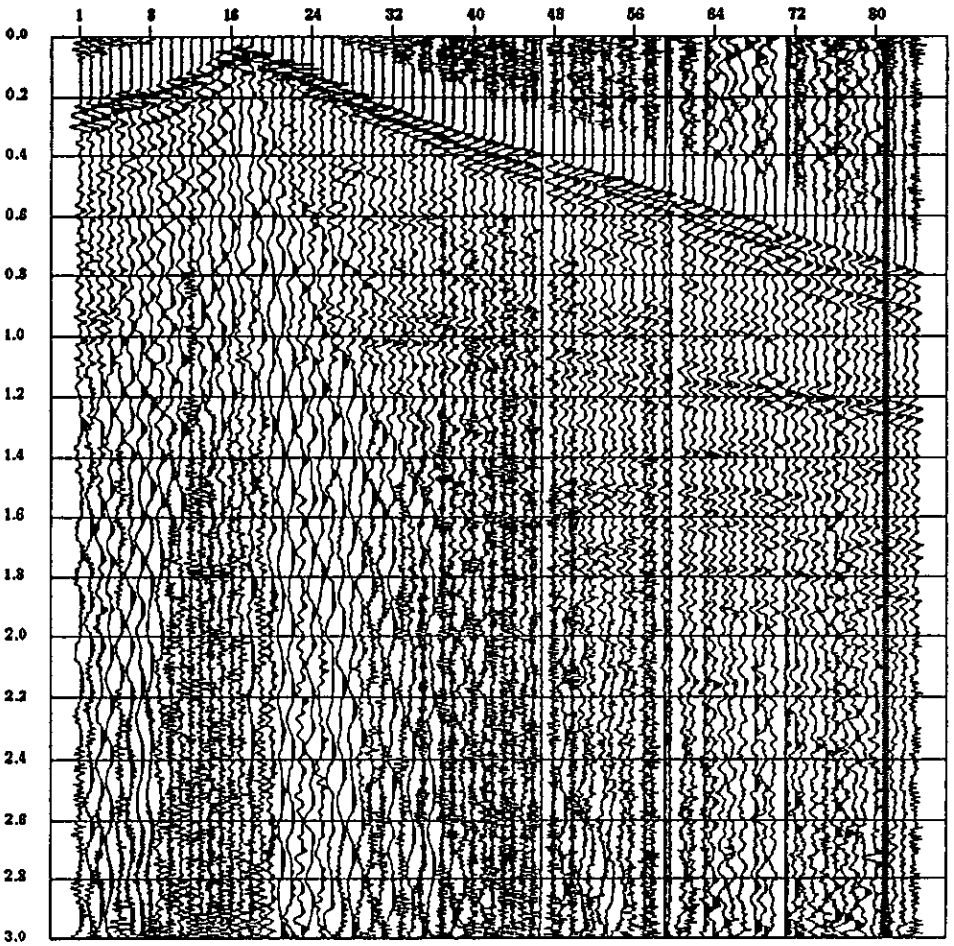

FIG 13. The vertical component of Rumsey data.